Scientific Research Publishing

American Journal of Climate Change, 2026, 15(3), 202-228
https://www.scirp.org/journal/ajcc
ISSN Online: 2167-9509
ISSN Print: 2167-9495

WorldClim-Based Mapping of Reference Evapotranspiration and Drought Conditions under Future Climate Scenarios in Al-Madinah Region, Saudi Arabia

Ohood Alharbi

Department of Geography and GIS, Faculty of Arts and Humanities, King Abdulaziz University, Jeddah, Saudi Arabia
Email: oaralharbi@kau.edu.sa

How to cite this paper: Alharbi, O. (2026). WorldClim-Based Mapping of Reference Evapotranspiration and Drought Conditions under Future Climate Scenarios in Al-Madinah Region, Saudi Arabia. *American Journal of Climate Change, 15,* 202-228.
https://doi.org/10.4236/ajcc.2026.153010

Received: August 12, 2026
Accepted: September 13, 2026
Published: September 16, 2026

Copyright © 2026 by author(s) and Scientific Research Publishing Inc.
This work is licensed under the Creative Commons Attribution International License (CC BY 4.0).
http://creativecommons.org/licenses/by/4.0/
Open Access

Abstract

Reference evapotranspiration (ET_0) and drought variability serve as critical indicators for comprehending climatic conditions in arid and semi-arid regions. This study assesses the efficacy of global climate model (GCM) outputs, compiled in the WorldClim open-access climate dataset, for estimating ET_0 and supporting standardised precipitation evapotranspiration index SPEI drought analysis in the Al-Madinah region. Monthly WorldClim temperature and precipitation data were initially compared with recorded historical station data (1970-2018) to evaluate accuracy. The results showed strong to very strong agreement, with R values ranging from 0.937 to 0.999 and R^2 values ranging from 0.878 to 0.999, although slight underestimation was observed for both temperature and precipitation. Then WorldClim-derived Hargreaves ET_0 was validated against station-based FAO-56 Penman-Monteith and station-based Hargreaves ET_0, also showing strong agreement. Future ET_0 was projected under SSP2-4.5 and SSP5-8.5 scenarios for four 20-year periods: 2021-2040, 2041-2060, 2061-2080, and 2081-2100. The projections indicated a gradual increase in ET_0 under both SSP scenarios, with stronger increases under SSP5-8.5, especially during 2081-2100. In this period, SSP5-8.5 showed an average monthly ET_0 of about 182.47 mm/month, equivalent to 2189.7 mm/year, representing an increase of 359.70 mm/year relative to the historical baseline. Baseline ET_0 was higher in the eastern and southeastern areas and lower in the northwest. Future projections showed the same spatial pattern, with increasing ET_0 values across the region, especially under SSP5-8.5 in the late century. SPEI projections indicated a shift from near-normal conditions in the early century to increasing moisture deficit after mid-century, particularly under SSP5-8.5. These results highlight the value of WorldClim-based climate projections for assessing climate variability, future climate-change impacts, drought susceptibility, and evaporative conditions, particularly in arid and semi-arid regions.

Keywords

WorldClim, Climate Change, Reference Evapotranspiration, SPEI, SSP2-4.5, SSP5-8.5

1. Introduction

Evapotranspiration (ET_0) refers to the total water movement from the land to the atmosphere, resulting from soil and surface water evaporation and plant transpiration (Zhang et al., 2020). It plays an essential role in the hydrological cycle and has significant implications for managing water resources, supporting agriculture, and promoting environmental sustainability, particularly in regions experiencing water stress, deficits, and climatic fluctuations (Hodam et al., 2017; Gharbia et al., 2018). Moreover, while evapotranspiration is regarded as the main factor influencing the hydrological budget after rainfall, accurately estimating its magnitude is viewed as being highly difficult due to the complex interactions between meteorological variables and the unique characteristics of each site (Gharbia et al., 2018). ET_0 is typically estimated using meteorological data from ground stations, including temperature, solar radiation, wind speed, and relative humidity. However, in many regions, particularly in developing countries, these networks are often sparse and frequently lack long, continuous, or complete records. As a result, this limitation hinders the ability to perform robust ET_0 calculations. In such cases, open-access climate products like WorldClim offer a powerful alternative by providing high-resolution gridded climate layers derived from global observation and modelling systems (Fick & Hijmans, 2017). These datasets supply consistent spatially explicit fields of temperature, precipitation, and related variables, enabling ET_0 estimation even where in situ measurements are limited or absent.

WorldClim provides future climate projections based on downscaled outputs from various general circulation models (GCMs) under different emission scenarios, enabling their use in spatial and ecological modelling (WorldClim, 2020b). For WorldClim v2.1, future climate layers are available for multiple CMIP6 GCMs and SSPs, with the present climate as the baseline for downscaling and debiasing. This would help evaluate how future climate change might affect evapotranspiration regimes and water demands across regions and time frames.

Many models and equations have been formulated to help estimate evapotranspiration. These equations differ in terms of data requirements, climatic variables, and complexity (Gharbia et al., 2018; Feng et al., 2016). The most prominent of these methods are Penman-Monteith, Priestley-Taylor, Makkink, Blaney-Criddle, and Hargreaves (Gharbia et al., 2018). In reviewing the literature, several studies have attempted to model the spatial distribution of ET_0 and examine the efficacy of ET_0 methods. ElNesr et al. (2010), Elnesr & Alazb (2013), and Salahudin et al.

(2023) applied ground meteorological data to estimate and visualize reference evapotranspiration (ET_0) (Penman-Monteith formula) spatially over several decades. El-Nesr et al. (2010) and Elnesr & Alazb (2013) found that ET_0 in Saudi Arabia was lowest in winter and highest in summer, with regional differences showing lower values in the southern region during cooler months and lower values in the western region during warmer months. Salahudin et al. (2023) indicated that the ensemble machine learning model achieved high performance in predicting ET_0 in Pakistan. Gharbia et al. (2018) have also used climatological observations to assess the efficacy of six algorithms for ET_0 by integrating with GIS in Ireland. The most accurate ET_0 model was combined with GCM ensembles of climate change models to predict future change influences on ET_0 amount in periods 2020, 2050, and 2080 under RCP 4.5 and RCP 8.5 scenarios. The results have revealed that the Hamon approach was the highest performer. The most significant increase in ET_0 is expected to be under the RCP 8.5 scenario at the end of the century in 2080, compared to 2020.

More recently, the use of gridded climate datasets, such as WorldClim, has become increasingly popular for estimating ET_0 in areas lacking dense meteorological networks. Zhang et al. (2020) used high-resolution climate data from the global datasets WorldClim v2.0 (1970-2000) and CHELSA v1.2 (1979-2013) to estimate evapotranspiration in the Urabá region of Colombia. WorldClim showed high accuracy in temperature representation, while CHELSA performed better in capturing rainfall. The Hargreaves and Thornthwaite methods delivered the most accurate streamflow estimates based on water balance analysis. Ezz and Abdelwares (2025) also utilized WorldClim v2 data (1970-2000) to calculate monthly reference evapotranspiration (ET_0) using the FAO Penman-Monteith equation integrated with GIS tools. The resulting maps offered a detailed spatial resolution, supporting more efficient irrigation planning and managing agricultural water needs. These studies highlight the usefulness of gridded climate datasets, particularly WorldClim, for mapping precipitation, evapotranspiration, and related climate variables in data-limited regions. Lemenkova (2022) demonstrated that global climate datasets can effectively capture spatial variation in evapotranspiration, vapour pressure deficit, and climatic water deficit across Ethiopia's complex topography, supporting the identification of areas with high atmospheric water demand and potential drought stress. Similarly, Bastidas Osejo et al. (2019) found that WorldClim performed well in representing temperature and precipitation patterns in the Urabá region of Colombia, especially when integrated with station data via spatial interpolation.

Although the use of WorldClim data for estimating reference evapotranspiration (ET_0) has become increasingly common, its application in semi-arid and arid regions remains relatively limited, particularly for future projections under climate change scenarios. This highlights the need for more ET_0 modelling efforts that utilise open-access climate datasets, such as WorldClim, to support decision-making in areas with limited climate monitoring capabilities. Therefore, this study aims to assess the efficacy of WorldClim open-access climate data for evapotranspiration mapping by analysing maximum and minimum temperature, precipitation, and potential evapotranspiration derived from temperature-based variables, and producing spatial evapotranspiration maps. It also examines projected ET_0 and SPEI under SSP2-4.5 and SSP5-8.5 scenarios across four future 20-year periods. This study contributes by developing a reproducible geospatial framework for assessing baseline and future reference evapotranspiration ET_0 and SPEI-based drought conditions using open-access WorldClim climate data. This would provide a spatially explicit and reproducible approach for assessing evaporative conditions and drought variability in a data-limited arid environment.

2. Data and Methodology

2.1. Study Area

The Al-Madinah region is located in the western part of Saudi Arabia between latitude 24˚28"N and longitude 39˚36"E (**Figure 1**). Geologically, the area lies within the Arabian Shield, which dates back to the Precambrian era (Subyani & Al-Ahmadi, 2011). Al-Madinah's geology has three main components: basaltic lava plateaus called Harrats; alluvial deposits of poorly sorted sand and gravel; and rocky outcrops in the west and north, seen as large massifs and small isolated outcrops (Gutub, 2013; Al-Shaibani et al., 2007). The study area is generally characterised by low rainfall, where the annual average does not exceed 122 mm/y and is primarily concentrated in the highlands, and the annual mean temperature in Al-Madinah was 27.73˚C with a maximum of 35.60˚C and a minimum of 19.89˚C (Alharbi, 2024). Al-Madinah ranks as the fourth largest region in Saudi Arabia in terms of population and urban development. According to data from the Saudi Central Department of Statistics and Information (GASTAT, 2010), the city's population was approximately 2,137 million in 2022.

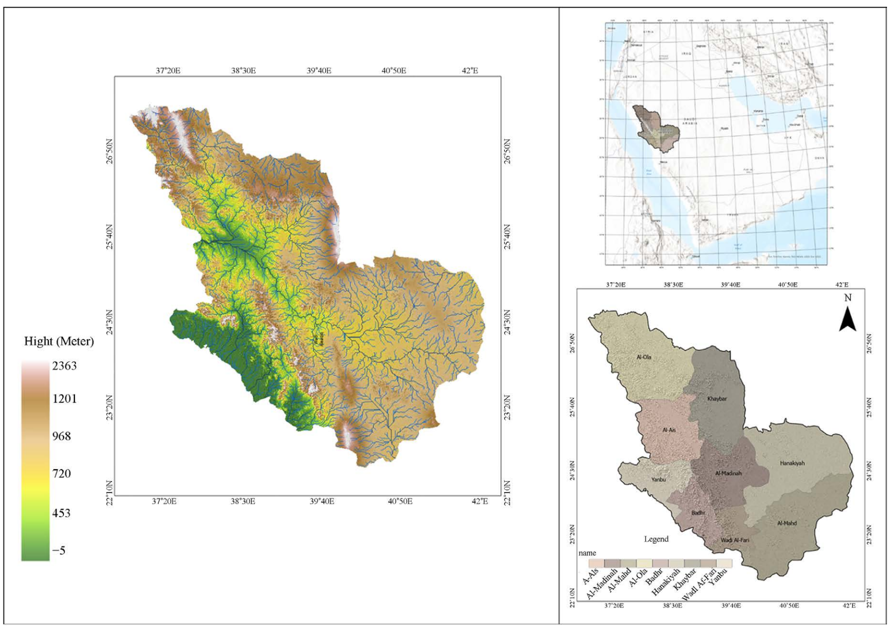

Figure 1. Study location and topographic characteristics of the study area.

2.2. Climate Data and Variables

The present study employed climate projections obtained from global climate models participating in the Coupled Model Intercomparison Project Phase 6 (CMIP6) through the WorldClim 2.1 dataset (**Figure 2**). CMIP6 projections are commonly used in Intergovernmental Panel on Climate Change (IPCC) assessments and are driven by Shared Socioeconomic Pathway (SSP) scenarios, which combine assumptions about socioeconomic development with specified levels of radiative forcing. The WorldClim CMIP6 dataset provides projections under four SSP scenarios: SSP1-2.6, SSP2-4.5, SSP3-7.0, and SSP5-8.5, representing sustainability-oriented low-emissions, middle-of-the-road, regional-rivalry, and fossil-fuel-intensive high-emissions pathways, respectively (Tarawneh & Chowdhury, 2018; WorldClim, 2020b). The data of CMIP6 have been downscaled and calibrated from CRU-TS-4.03 by the Climatic Research Unit, University of East Anglia, using WorldClim 2.1 for bias correction (WorldClim, 2020a). The predictions of precipitation and temperature in two scenarios, high emissions (SSP5-8.5) and medium stabilisation (SSP2-4.5), were used. These data have been designed in monthly means for 20-year periods that could be divided into near future (2021-2040), far future that includes mid-century (2041-2060 and 2061-2080), and end-century (2081-2100). They have a spatial resolution of 2.5 minutes or about ~21 km^2 at the equator (Harris et al., 2014; Fick & Hijmans, 2017). The baseline period data were selected from 1970 to 2018 from historical climate data in WorldClim. The monthly values of future projections of total precipitation (mm), maximum temperature (˚C), and minimum temperature (˚C) have been derived from four global climate models (GCMs), namely BCC-CSM2-MR, CNRM-CM6-1, CanESM5, and IPSL-CM6A-LR (**Table 1**). These GCM models were selected because they are commonly used and the models showed acceptable performances (McSweeney et al., 2014), including studies of future climate change over the Arabian Peninsula and historical precipitation simulations over Africa and the Arabian Peninsula (Almazroui et al., 2020; Nooni et al., 2023). Raster resolution, spatial extent, coordinate reference system, and cell alignment were verified before conducting pixel-based analysis.

Table 1. Basic information about the selected CMIP6-GCMs models.

GCMs Models	Institute/Country	Resolution (Lat × Lon)
BCC-CSM2-MR	Beijing Climate Center Climate System Model, China	$1.125^0 \times 1.125^0$
CNRM-CM6-1	Centre National de Recherches Météorologiques, France	$1.4^0 \times 1.4^0$
CanESM5	Canadian Center for Climate Modeling and Analysis, Canada	$2.8^0 \times 2.8^0$
IPSL-CM6A-LR	Institute of Pierre Simon Laplace (IPSL), France	$1.26^0 \times 1.26^0$

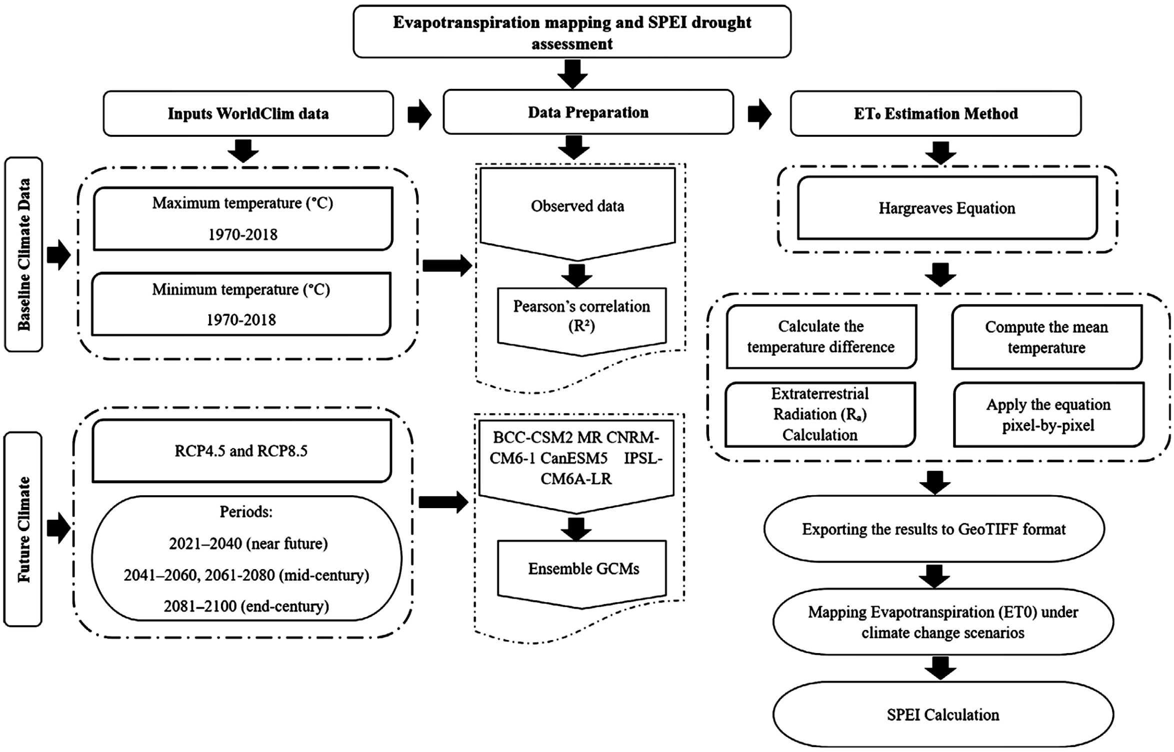

Figure 2. Flowchart of study methodology.

2.3. Historical Evaluation of WorldClim Data

The performance of the WorldClim historical climatology (1970-2018) was evaluated against the observed monthly climatology (1973-2018) using four statistical metrics: the mean absolute error (MAE), root mean square error (RMSE), Pearson correlation coefficient (r), and coefficient of determination. These metrics were selected to capture average error magnitude, sensitivity to large deviations, and consistency in seasonal patterns. The mean absolute error was calculated as:

$$MAE = \frac{1}{n}\sum_{i=1}^{n}\left[S_i - O_i \right] \tag{1}$$

where S_i is the WorldClim value for month i, O_i is the corresponding observed value, and n is the number of monthly observations. MAE represents the average absolute difference between the two datasets and is expressed in the original unit of the evaluated variable. It therefore provides a direct and readily interpretable measure of the typical monthly error.

RMSE also measures the magnitude of the differences between WorldClim and observations, but it assigns greater weight to relatively large errors because the deviations are squared before averaging. This metric was therefore employed to determine if months with particularly large discrepancies adversely affected the agreement between the two datasets. This analysis aimed to identify whether months with particularly large discrepancies adversely affected the agreement between the two datasets. Both MAE and RMSE approach zero as agreement improves (Hodson, 2022). The root mean square error was computed as:

$$RMAE = \sqrt{\frac{1}{n}\sum_{i=1}^{n}\left(S_i - O_i\right)} \tag{2}$$

The Pearson correlation coefficient was used to assess the strength of the linear relationship between the observed and WorldClim monthly climatology:

$$r = \frac{\sum_{i=1}^{n}\left(O_i - \bar{O}\right)\left(S_i - \bar{S}\right)}{\sqrt{\sum_{i=1}^{n}\left(O_i - \bar{O}\right)^2 \sum_{i=1}^{n}\left(S_i - \bar{S}\right)^2}} \tag{3}$$

where $\bar{O}$ and $\bar{S}$ are the mean observed and WorldClim values, respectively. The coefficient ranges from −1 to +1 (Profillidis & Botzoris, 2019), with values approaching +1 indicating that WorldClim closely reproduces the seasonal variation of the observed climatology. Because correlation evaluates correspondence in pattern rather than absolute agreement, it was interpreted together with the error-based metrics. The coefficient of determination was calculated as:

$$R^2 = r^2 \tag{4}$$

and was used to express the proportion of the observed monthly variability associated with the linear relationship between the WorldClim and observed datasets. Values approaching 1 indicate strong correspondence in the seasonal climatic cycle. Monthly bias was calculated as the difference between the WorldClim historical value and the corresponding observed value, following the conventional model-minus-observation approach used in climate-data evaluation.

2.4. Multi-Model Ensemble Construction

The multi-model ensemble (MME) approach was calculated as the arithmetic mean of the selected GCM outputs for each grid cell, scenario, and future period. This approach helps reduce the influence of individual model uncertainty and provides a more robust representation of projected climate conditions than reliance on a single GCM (Jose et al., 2022; Ahmed et al., 2020).

$$MME_i = \frac{1}{M}\sum_{m=1}^{M} X_{m,i} \tag{5}$$

where $X_{m,i}$ is the value from model m at grid cell i, and $M = 4$ is the number of climate models.

2.5. Reference Evapotranspiration (ET_0)

The Hargreaves approach is chosen in the present study due to its requirement of fewer variables, the minimum and maximum temperature, and extraterrestrial radiation (Ra) (Čadro et al., 2017). All these variables are available in the WorldClim dataset. The WorldClim dataset (1970-2018) has been processed by the raster package as well as the libraries' rgdal and geosphere to extract the Eto-related maps. The code used is adapted from codes created by Spencer (2013b, 2013a). Hargreaves' equation is applied as:

$$ET_0 = 0.0023\left(0.408\right)\left(Tmean + 17.8\right)\left(TMax - TMin\right)0.5Ra \tag{6}$$

where ET_0 is Evapotranspiration Potential (mm/month); 0.0023 is an empirical coefficient used for unit conversion that also includes the kRs as an adjustment factor for solar radiation, and 0.408 is a factor to convert MJ m^{-2} to mm. Tmax = maximum air temperature (˚C), Tmin = minimum air temperature (˚C), Ra = extraterrestrial radiation in mm/day (Fisher & Pringle III, 2013; Čadro et al., 2017). Reference evapotranspiration was estimated using the Hargreaves method based on monthly maximum, minimum, and mean temperature data. The calculation was applied on a pixel-by-pixel basis in the R environment to produce monthly ET_0 raster layers. The monthly ET_0 layers were then aggregated to derive the annual baseline ET_0.

2.6. ET_0 Validation

The validation of the reliability of the baseline WorldClim-derived reference evapotranspiration (ET_0) was conducted using two approaches. The first approach included a comparison between the Hargreaves ET_0 derived by WorldClim and the station-based ET_0 calculated using the FAO-56 Penman-Monteith method. The standard reference method was selected as the FAO-56 Penman-Monteith method due to its comprehensive examination of the primary meteorological factors that influence evapotranspiration, including air temperature, solar radiation, wind speed, vapour pressure, and atmospheric pressure. Additionally, this method proves to be beneficial in arid, temperate, and tropical regions (Delgado-Ramirez et al., 2023). The objective of this comparison was to directly assess the reliability of the WorldClim-derived ET_0 in comparison to a physically grounded station reference. The FAO-56 Penman-Monteith equation for reference evapotranspiration (ET_0) is:

$$ET_0 = \frac{0.408\Delta\left(R_n - G\right) + \gamma \frac{900}{T+273} u_2 \left(e_s - e_a\right)}{\Delta + \gamma\left(1 + 0.34u_2\right)} \tag{7}$$

where ET_0 is reference evapotranspiration (mm day^{-1}), R_n is net radiation at the crop surface (MJ m^{-2} day^{-1}), G is soil heat flux density (MJ m^{-2} day^{-1}), T is mean air temperature at 2 m height (C), u2 is wind speed at 2 m height (m s^{-1}), es is saturation vapor pressure (kPa), ea is actual vapor pressure (kPa), $e_s - e_a$ is vapor pressure deficit (kPa), Delta is the slope of the saturation vapor pressure curve (kPa C^{-1}), and gamma is the psychrometric constant (kPa C^{-1}) (Moratiel et al., 2020). For monthly calculations, daily ET_0 was converted to monthly total ET_0 as:

$$ET_{0,monthly} = ET_{0,daily} \times N \tag{8}$$

where N is the number of days in the month.

The second approach compared the Hargreaves ET_0 from WorldClim with the station-based Hargreaves ET_0. This comparison aimed to provide methodologically consistent validation, as the spatial ET_0 maps generated in this study also used the Hargreaves method. Using the same ET_0 equation for both WorldClim and station data enables a more precise distinction between uncertainties from the input climate data and those arising from differences among ET_0 methodologies.

In addition, inter-model consistency of projected reference evapotranspiration (ET_0) was evaluated for the four selected CMIP6 GCMs—BCC-CSM2-MR, CNRM-CM6-1, CanESM5, and IPSL-CM6A-LR—prior to calculating the multi-model ensemble mean. Pairwise Pearson correlation coefficients of monthly ET_0 projections were calculated separately for each scenario and 20-year future period to assess agreement in the monthly ET_0 pattern among the models. Inter-model spread in projected ET_0 magnitude was quantified using the coefficient of variation (CV), calculated as the standard deviation of model projections divided by their ensemble mean. Lower CV values indicate stronger inter-model agreement, whereas higher values indicate greater projection uncertainty. This assessment provides an indication of the consistency and uncertainty of individual-model projections before their use in the multi-model ensemble mean.

2.7. The Standardized Precipitation Evapotranspiration Index (SPEI)

Calculating ET_0 rates enables better monitoring of drought conditions and water resources in Al-Madinah by integrating evapotranspiration estimates with precipitation data. Consequently, the standardized precipitation evapotranspiration index (SPEI) is considered a beneficial index to show the impacts on the hydrological system and water resources by linking these ET_0-based estimates with the temporal pattern of drought events and by providing a good understanding of the water surplus or deficit cases during the period investigated (Faye et al., 2019; Qaisrani et al., 2021). The SPEI is formulated based on the monthly climatic water balance and is usually represented by calculating the difference between precipitation and evapotranspiration (Abdullah, 2014). The monthly climatic water balance over a specified time period (D_i) is calculated:

$$D_i = P_i - PET_i \tag{9}$$

where P_i stands for the amount of precipitation, and PET_i represents Potential Evapotranspiration for the same month "I". The negative value between quantities of rain and ET_0 often indicates an existing rainfall deficit (RD), whereas surplus (RS) occurs when rainfall is more than evapotranspiration (Feng et al., 2016). The SPEI index included the aggregation of D_i values in different time scales, such as 1-month or 6-month periods. This aggregation is then converted into standardizing values using the log-logistic distribution that represents how many standard deviations a D_i value is from the mean of the log-logistic distribution. This provides a consistent method for comparing and interpreting drought or wet conditions across different periods and regions. The mathematical representation of the probability density function for the log-logistic distributed variable is as follows:

$$f_{(x)} = \frac{\beta}{\alpha}\left(\frac{x \backsim y}{a}\right)^{\beta-1}\left[1+\left(\frac{x \sim y}{a}\right)^{\beta}\right]^{-2} \tag{10}$$

where α, β, and γ are scale, shape, and origin parameters respectively (Vicente-

Serrano et al., 2010; Qaisrani et al., 2021). The Log-logistic distribution adopted for standardizing the D series for all time scales is given by:

$$f_{(x)} = \left[1 + \left(\frac{a}{x} - y\right)^{\beta}\right]^{-1} \tag{11}$$

$f(x)$ value is then transformed to a normal variable by means of the following approximation:

$$SPEI = W - \frac{c_0 + c_1 w + c_2 w^2}{1 + d_1 w \ + d_2 w^2 + d_3 w^3} \tag{12}$$

where $P = 1 - f(x)$, and W is given by

$$w = \begin{cases} \sqrt{-21n}\,(P) & if \ p \le 0.5 \\ \sqrt{-21n}\,(1-p) & if \ \ge 0,5 \end{cases} \tag{13}$$

where C_0, C_1, C_2, d_1, d_2, and d_3 are constants equal to 2.515517, 0.802853, 0.010328, 1.432788, 0.189269, and 0.001308, respectively (Vicente-Serrano et al., 2010). Moreover, the drought and moisture conditions would be identified via the SPEI values as displayed in **Table 2**. These values range from positive, meaning wet conditions, to negative values that exhibit drought events, while the SPEI value indicates the event's intensity (Mohammed & Algarni, 2020). Therefore, drought years were identified with the threshold values of −1 (Driouech et al., 2020; McKee et al., 1993).

Table 2. The degree of drought and moisture in SPEI.

SPEI Values	Conditions
SPEI ≤ −2	Extreme Drought
−2 < SPEI ≤ −1.5	Severe Drought
−1.5 < SPEI ≤ −1	Moderately Drought
−1 < SPEI ≤ 1	Near Normal
1 < SPEI ≤ 1.5	Moderately Wet
1.5 < SPEI ≤ 2	Severely Wet
SPEI ≥ 2	Extremely Wet

The SPEI includes multiple timescales that exemplify different types of droughts. Short timescales are more suitable for detecting meteorological drought and agricultural drought, which are (1 - 3 months averages) and (3 - 6 months averages). The long-time scales often used for hydrological drought and water resources average (12 to 24 months averages) (Pei et al., 2020; Abdullah, 2014; Faye et al., 2019). In order to produce the SPEI index for the study area, the values of historical ET_0 (1970-2018) and future (2021-2100) have been extracted from the maps generated based on the Worldclim database, utilising the climate station's locations in Al-Madinah, which are 40430, 40439, M001, M002, and M004.

3. Results and Dissection

3.1. Historical Validation of the WorldClim Climatology

The accuracy assessment indicates that WorldClim temperature data showed strong agreement with the observed station records for all temperature variables (Table 3 and Figure 3). The correlation coefficients were notably high, ranging from 0.998 to 0.999, indicating that WorldClim effectively captured the seasonal variation of maximum, minimum, and mean temperature. However, the error statistics reveal some differences in accuracy among the variables. The minimum temperature had the best performance, with the lowest RMSE and MAE values, with RMSE = 0.955˚C and MAE = 0.733˚C. In contrast, maximum temperature showed the largest error, with RMSE = 2.010˚C and MAE = 1.939˚C. The mean temperature showed intermediate error values, reflecting the combined influence of both minimum and maximum temperature estimates. The bias results showed that WorldClim generally underestimated observed temperatures, as indicated by negative bias across all variables. This underestimation was more pronounced for maximum temperature, while minimum temperature showed the smallest bias. The monthly bias pattern further confirms that the magnitude of underestimation varied throughout the year, with larger differences occurring during some cooler months (Figure 3). The precipitation dataset showed strong agreement between WorldClim and observed records, with R = 0.937 and R^2 = 0.878 (Table 3 and Figure 3), indicating that WorldClim captured most monthly precipitation variability. The bias value was slightly negative (−0.332 mm), indicating a small overall underestimation by WorldClim. Monthly bias patterns showed that WorldClim overestimated precipitation mainly in March and April, while it underestimated precipitation in most other months, as shown in Figure 3. Overall, the precipitation data showed acceptable performance, but with lower reliability than the temperature data.

Table 3. Accuracy assessment of WorldClim temperature and precipitation data against observed station records.

Variable	R	R^2	RMSE	MAE	Bias
Tmax ˚C	0.998	0.995	2.010	1.939	−1.939
Tmin ˚C	0.999	0.999	0.955	0.733	−0.628
Tmean ˚C	0.999	0.999	1.394	1.286	−1.284
Precipitation mm	0.937	0.878	2.038	1.585	−0.332

The study area is characterised as a dry region, experiencing intense summer heating and limited rainfall that is concentrated in certain seasons. Temperatures, as shown in Figure 4, rise gradually from winter to summer, with maximum (Tmax), minimum (Tmin), and mean (Tmean) temperatures peaking during July and August before declining towards the winter months. This pattern illustrates the presence of hot summers and relatively cooler winters. Conversely, precipitation exhibits a highly seasonal and irregular distribution, with the majority of rainfall occurring in March to April and November to December, while there is very low precipitation during the summer months, particularly from June to September (**Figure 4**). These climatic characteristics provide an important basis for interpreting the temporal and spatial distribution of ET_0. Therefore, WorldClim-based ET_0 estimation allows the baseline spatial distribution and future changes of ET_0 to be assessed consistently, which also supports the later interpretation of SPEI-based drought conditions.

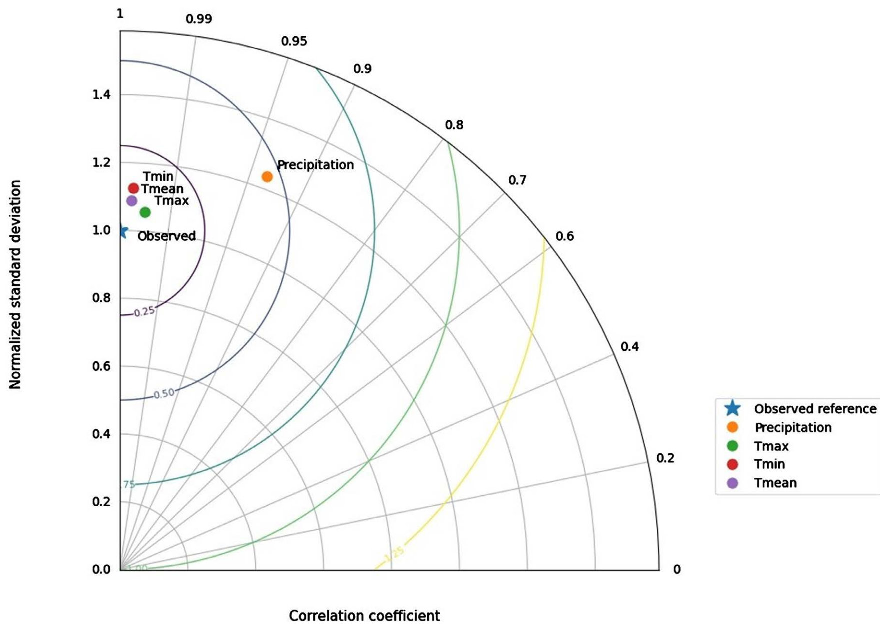

Figure 3. Taylor diagram evaluating the agreement between the WorldClim historical climatology and observed monthly climate data. The diagram summarizes Pearson's correlation coefficient, normalized standard deviation, and normalized centered root mean square (RMSD) difference. Variables positioned closer to the observational reference point exhibit stronger agreement with the observed climatology.

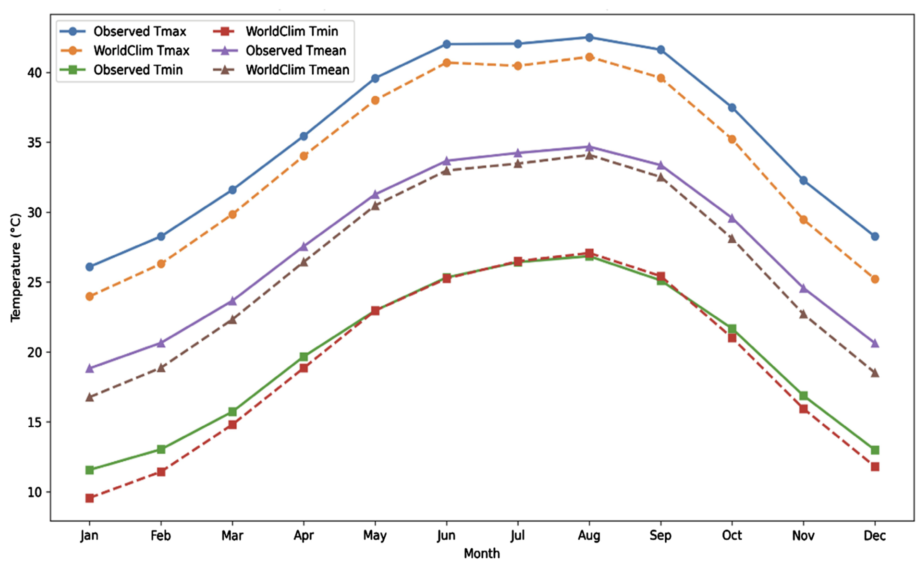

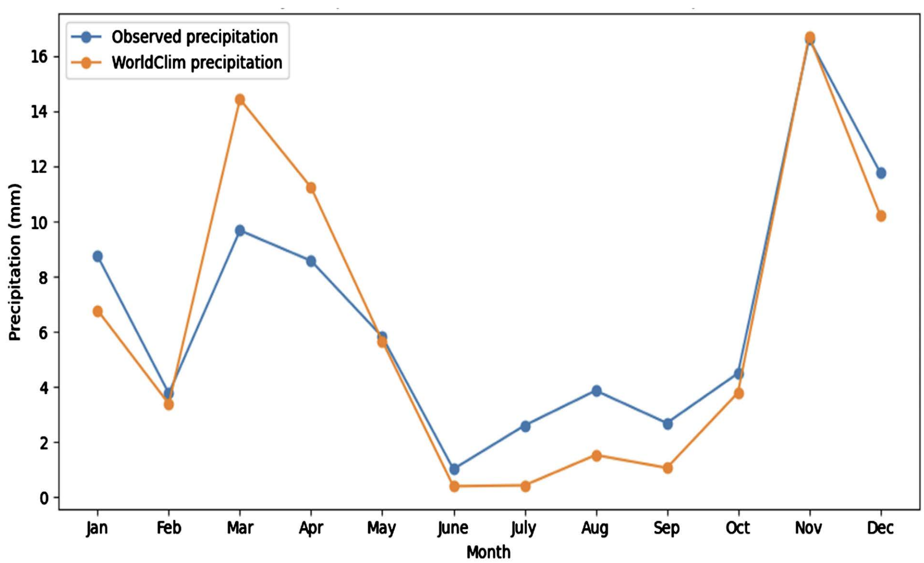

Figure 4. Monthly comparison between observed and WorldClim climate variables in Al-Madinah.

3.2. Validation of WorldClim-Derived ET_0 Estimates

The validation statistics are summarised in **Table 4** and **Figure 5**. WorldClim-derived ET_0 showed a strong correspondence with station-based FAO-56 Penman-Monteith ET_0, with R = 0.960 and R^2 = 0.921, indicating that the seasonal pattern of monthly evapotranspiration was well captured. Nevertheless, the relatively high RMSE (62.271 mm month^{-1}), MAE (59.124 mm month^{-1}), and negative bias (−59.124 mm month^{-1}) indicate underestimation of ET_0 magnitude relative to the FAO-56 reference. In contrast, a stronger and more consistent performance was obtained when WorldClim-derived ET_0 was evaluated against station-based Hargreaves estimates, for which the correlation increased to R = 0.975 (R^2 = 0.951), while RMSE and MAE decreased substantially to 11.911 and 10.089 mm month^{-1}, respectively. The small positive bias of 3.208 mm month^{-1} indicated that the WorldClim-derived estimates were closely aligned with the station-based Hargreaves values, with only slight overestimation. Overall, these findings indicated that the WorldClim-derived product can adequately represent local evapotranspiration dynamics. The particularly close correspondence with station-based Hargreaves-ET_0 further supports the reliability of WorldClim climatic data for estimating ET_0 at the local scale, while the larger differences relative to FAO-56 Penman-Monteith are likely associated primarily with methodological differences rather than with an inability of WorldClim data to reproduce local ET_0 variability.

The correlation analysis demonstrated strong agreement among the four selected CMIP6 GCMs in reproducing the seasonal pattern of projected Hargreaves ET_0. Under SSP2-4.5, the pairwise correlations remained consistently high across all future periods, indicating that the models produced highly similar monthly ET_0 patterns under the intermediate-forcing scenario. Under SSP5-8.5, the correlations were also generally high, but a wider range was observed during the late-century

Table 4. Statistical validation of WorldClim-derived Hargreaves ET_0 against station-based FAO-56 Penman-Monteith and station-based Hargreaves ET_0.

Metric	WorldClim Hargreaves ET_0 vs Station FAO-56 PM	WorldClim Hargreaves ET_0 vs Station Hargreaves ET_0
R	0.960	0.975
R^2	0.921	0.951
RMSE mm/month	62.271	11.911
MAE mm/month	59.124	10.089
Bias mm/month	−59.124	3.208

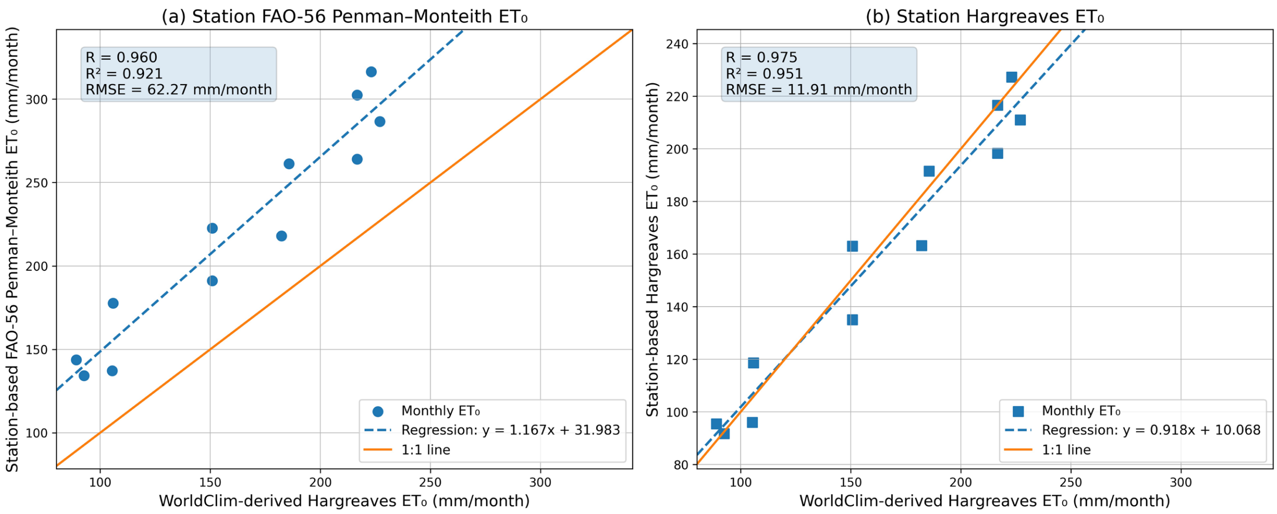

Figure 5. Linear relationships between WorldClim-derived Hargreaves ET_0 and station-based ET_0 references: (a) station-based FAO-56 Penman-Monteith ET_0 and (b) station-based Hargreaves ET_0. The dashed line represents the fitted regression line, while the solid line represents the 1:1 agreement line.

periods. Specifically, pairwise correlations ranged from 0.986 to 0.999 in 2021-2040, 0.963 to 0.998 in 2041-2060, 0.935 to 0.998 in 2061-2080, and 0.894 to 0.997 in 2081-2100. The lowest correlation values occurred mainly between CanESM5 and IPSL-CM6A-LR, particularly during 2081-2100, suggesting increased inter-model divergence under SSP5-8.5 toward the end of the century (Figure A1 and Figure A2). The coefficient of variation showed that the inter-model spread in projected ET_0 magnitude was generally low. Under SSP2-4.5, annual CV values ranged from 1.976% to 2.378%, reflecting close agreement among the four GCMs throughout the future periods. Under SSP5-8.5, CV values were higher, rising from 2.115% in 2021-2040 to 4.411% in 2081-2100, indicating greater projection spread under stronger climate forcing (Table A1). Nevertheless, the overall CV values remained relatively low, confirming that the multi-model ensemble mean can provide a good representative estimate of future ET_0 projections.

3.3. Spatial Distribution of Evapotranspiration under the Baseline Period and Future Scenarios

The baseline annual ET_0 map (Figure 6) showed clear spatial variability across the study area. Higher ET_0 values were mainly concentrated in warmer and lower-elevation areas, such as Wadi Al-Hamd and Al-Harrat in the middle, eastern, and southeast parts, while lower ET_0 values were observed in cooler or higher-elevation zones in the north and northwestern areas. This spatial pattern indicates that baseline ET_0 is strongly influenced by temperature gradients and topographic variation. The peak values were recorded during the summer months (June, July, and August), whereas the lowest rates occurred in winter, specifically in December and January, with November also noted, as illustrated in Figure 7. Moreover, the annual evapotranspiration rates of Al-Madinah show substantial amounts of increase across the years, ranging from 1493 to 2151 mm/year. There are similarities between the historical trend results of ET_0 in Al-Madinah in this study compared to those concluded by Elnesr and Alazb (2013), who investigated the ET_0 rate by applying the Food and Agriculture Organization (FAO) Penman-Monteith (PM) method in 29 meteorological stations distributed all over Saudi Arabia for the period 1980 to 2008. The findings revealed the highest amount of ET_0 in the summer and the lowest in the winter in the country's entirety. The annual evapotranspiration rate of Al-Madinah was high (2151 mm/year), a value also reported

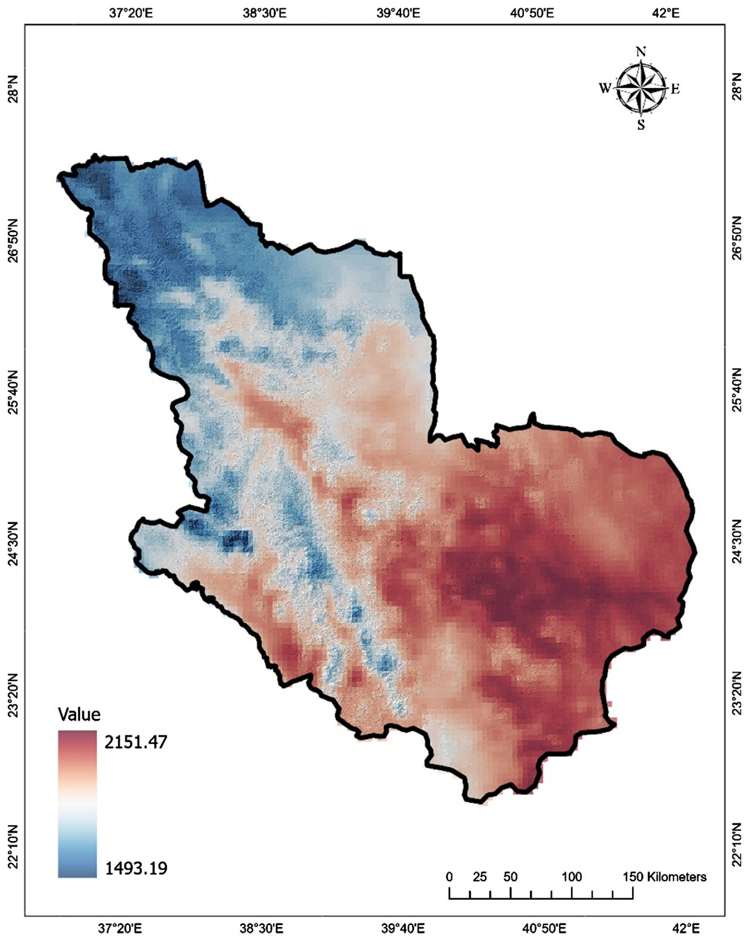

Figure 6. Spatial distribution of baseline annual reference evapotranspiration (1970-2018) in Al-Madinah.

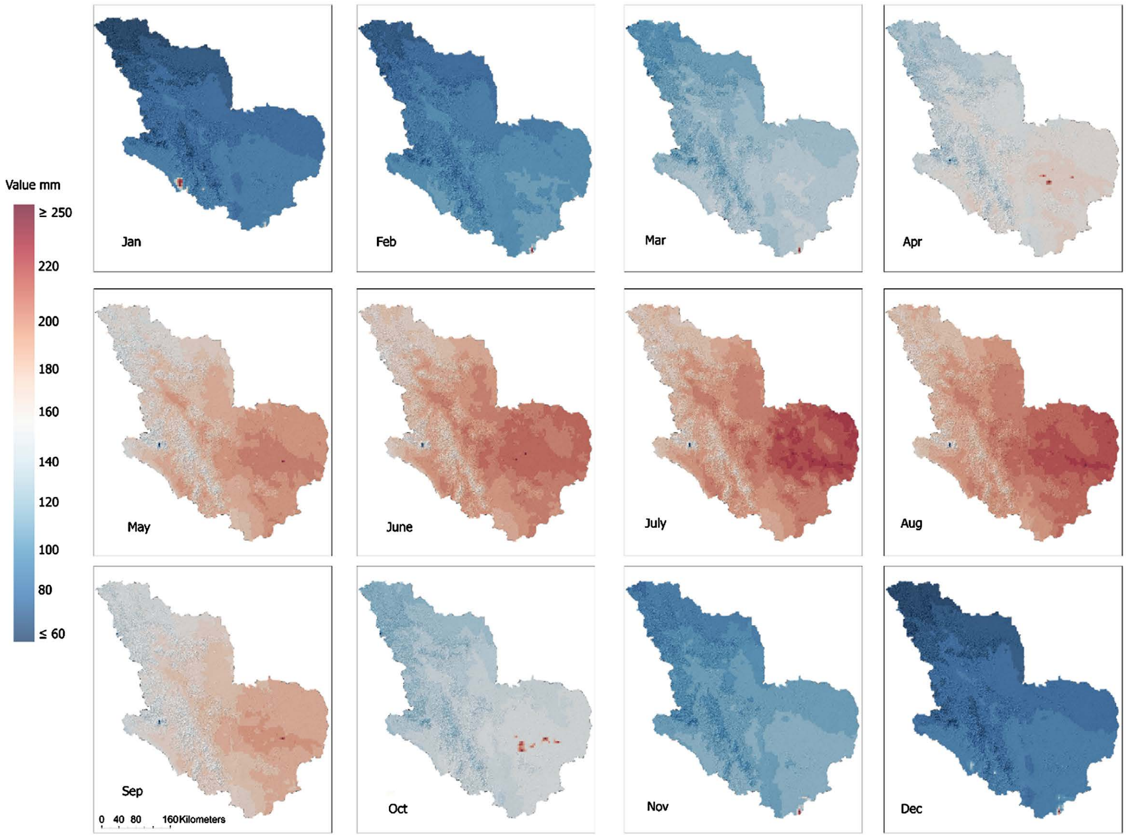

Figure 7. The spatial distribution of monthly averaged ET_0 in Al-Madinah (1970-2018).

by Mahmoud and Alazba (2016), and was slightly higher (ranging from 2059 to 2405 mm/year during 1992-2014). These values are often expected in arid and semi-arid regions such as Saudi Arabia. For example, the ET_0 amount of the central regions (Riyadh, Al-Qassim, Hail provinces) was estimated to be above 2100 mm/year from 1950 to 2013 (Mahmoud & Gan, 2019). These regions mostly experience marginally hotter temperatures than Al-Madinah.

In addition, the temperature will potentially rise steadily under both SSPs, with an average of about one degree Celsius per 20-year period in the near future (2021-2040) and the mid-century (2041-2060 and 2061-2080), with a more noticeable increase of around two degrees Celsius by the end of the century (2081-2100), in most months. These results agree with those obtained by Driouech et al. (2020), who concluded that the warming trend on the Arabian Peninsula is predicted to be larger under SSP5-8.5 (4˚C increases) than the SSP2-4.5 scenario (2˚C increases), an almost similar finding was also reported by Tarawneh and Chowdhury (2018), who estimated that the temperature is likely to rise gradually under SSP5-8.5 to around 1.3 - 1.6 C and 2.1 - 3.7 C by 2025-2044 and 2045-2064 periods, respectively, to reach a high point in 2065-2084 by increasing by 3.2 - 3.8 C.

The evapotranspiration rate increases in response to rising temperatures. This study's projections of future evapotranspiration closely align with temperature trends. Evapotranspiration is projected to increase steadily across all periods under both SSP2-4.5 and SSP5-8.5 scenarios, relative to the baseline period of 1970-2018. These increases will likely intensify later in the century, particularly from 2081 to 2100 and under the more extreme scenarios. For example, under SSP5-8.5, the increase is stronger. Mean monthly ET_0 rises from 166.07 mm/month during 2021-2040 to 182.47 mm/month during 2081-2100. The corresponding annual ET_0 increases from 1992.83 mm/year to 2189.68 mm/year, representing an increase of 8.90% to 19.66% relative to the historical baseline. This indicates a substantial intensification of atmospheric evaporative demand, especially under the late-century high-forcing scenario.

The most substantial increases are expected in summer months, reaching 18.93% by 2081-2100, while the winter months show smaller gains (**Figure 8**). This condition would also be similar to the winter across the Kingdom (MEIMR, 2016). A modest increase of up to 5% (9.7 mm) is anticipated in spring (April and May) under SSP5-8.5 during 2081-2100. This result is consistent with MEIMR (2016) estimations, which reported that the ET_0 rate of the Al-Madinah region is projected to increase slightly in the springtime, around 2% by 2080, more than other areas located in the southeast and southwest parts of Saudi Arabia. This study's projected trend in evapotranspiration agrees with the estimates of MEIMR (2016), which concluded that evapotranspiration would be higher in Saudi Arabia by the end of the 2080 period.

The spatial distribution of projected ET_0 shows a consistent pattern across all periods and scenarios (**Figure 9**). Under SSP2-4.5, the increase appears gradual from 2021-2040 to 2081-2100, with moderate expansion of higher ET_0 classes. Under SSP5-8.5, the increase is more pronounced, especially during 2061-2080

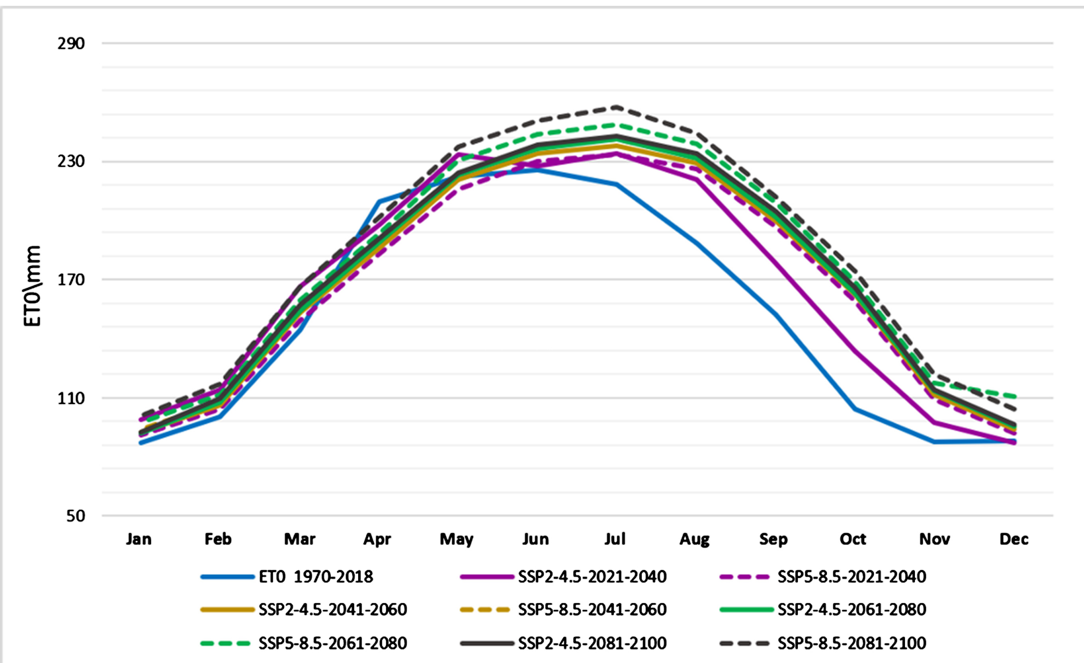

Figure 8. Projections of average evapotranspiration (ET_0)/mm, in Al-Madinah under SSP2-4.5 and SSP5-8.5 scenarios from 2021 to 2100.

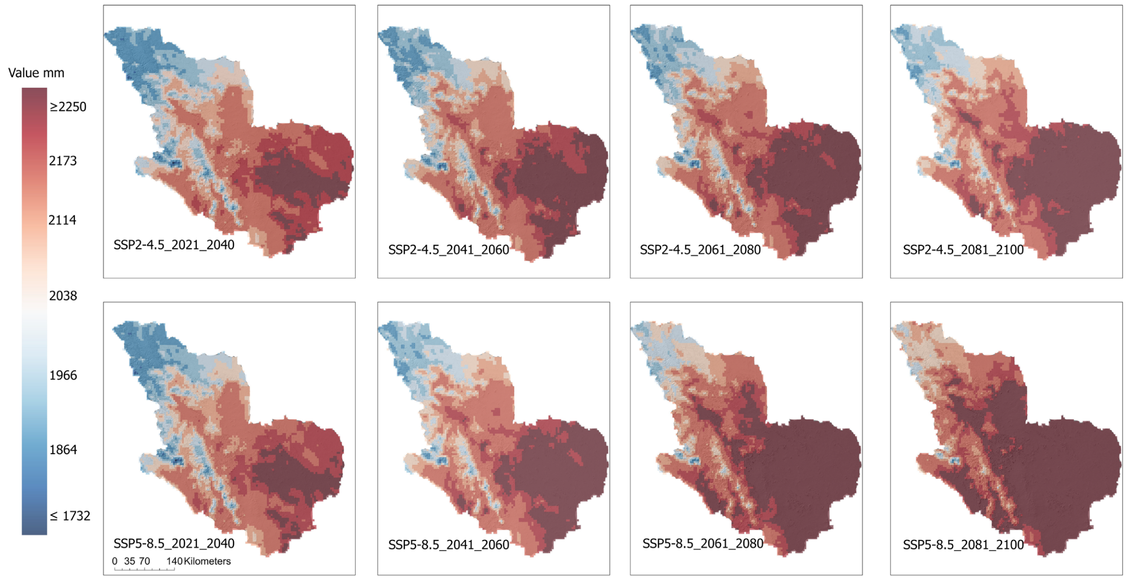

Figure 9. Spatial distribution of projected annual reference evapotranspiration (ET_0; mm/year) in Al-Madinah under SSP2-4.5 and SSP5-8.5 scenarios from 2021 to 2100.

and 2081-2100, when high ET_0 values become more widespread across the study area. This suggests that atmospheric water demand is expected to intensify more strongly under the high-emission scenario.

3.4. Projected Precipitation and Climatic Water Balance

Projected precipitation, Hargreaves ET_0, and climatic water balance were analysed under SSP2-4.5 and SSP5-8.5 for four future periods: 2021-2040, 2041-2060, 2061-2080, and 2081-2100. The results showed that annual precipitation is projected to increase moderately relative to the historical WorldClim baseline of 75.665 mm/year, with increases ranging from 10.97% to 12.80% (83.97 to 85.36 mm) under SSP2-4.5 and from 12.27% to 15.45% (84.95 to 87.36 m) under SSP5-8.5 (**Figure 10**). However, the projected increase in ET_0 is substantially larger than the increase in precipitation. Under SSP2-4.5, ET_0 increases from 1991 mm/year during 2021-2040 to 2072 mm/year during 2081-2100. Under SSP5-8.5, ET_0 increases more strongly, from 1992.8 mm/year to 2189 mm/year over the same period. As a result, the climatic water balance, calculated as precipitation minus ET_0, becomes increasingly negative under both scenarios, as shown in **Figure 11**. This indicates that projected precipitation gains are not sufficient to compensate for the increase in evaporative demand.

3.5. The Drought Conditions under SPEI

Al-Madinah could face drought events and water deficiency challenges caused by the increased ET_0 rate with reduced rainfall, negatively affecting the hydrological and water resources. The analysis of historical data for meteorological droughts by the SPEI index showed Al-Madinah was characterised by wetter conditions in the first half of the 20th century (1970-2000) than in the last half, which experienced more drought cases (Figure 12). These results are in agreement with those obtained by The National Centre of Meteorology in Saudi Arabia NCM (2019), which applied the Precipitation Index (SPI) to monitor drought situations (1985 to 2019 in 12-month); the findings have confirmed that there were moderate

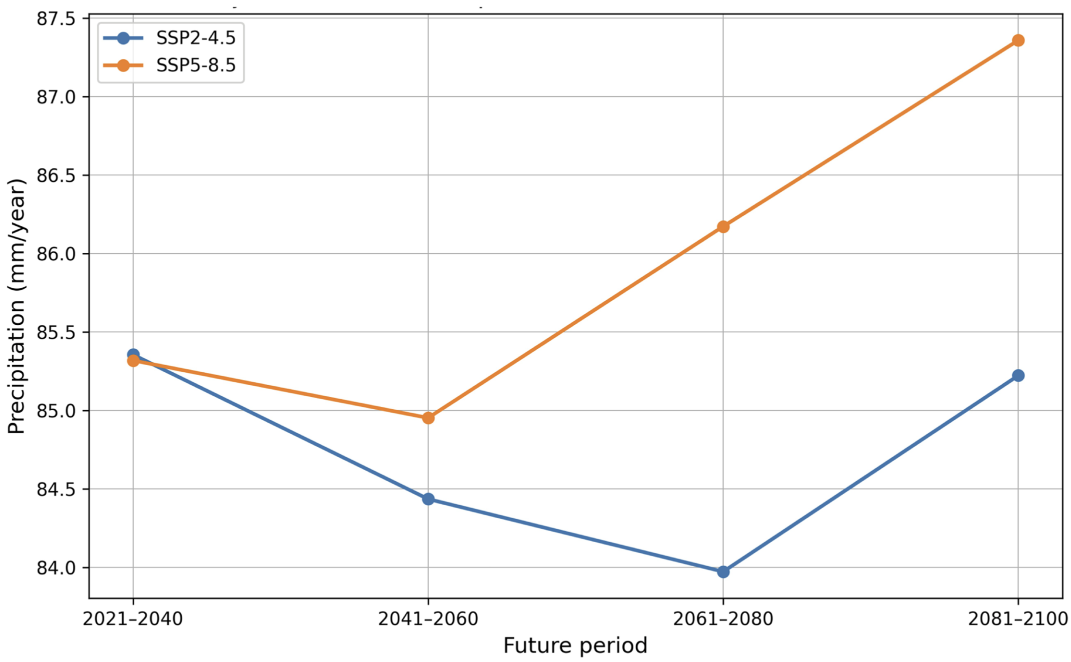

Figure 10. Projected annual precipitation under SSP2-4.5 and SSP5-8.5 for the periods 2021-2040, 2041-2060, 2061-2080, and 2081-2100. The figure shows moderate temporal and scenario-based variability in precipitation.

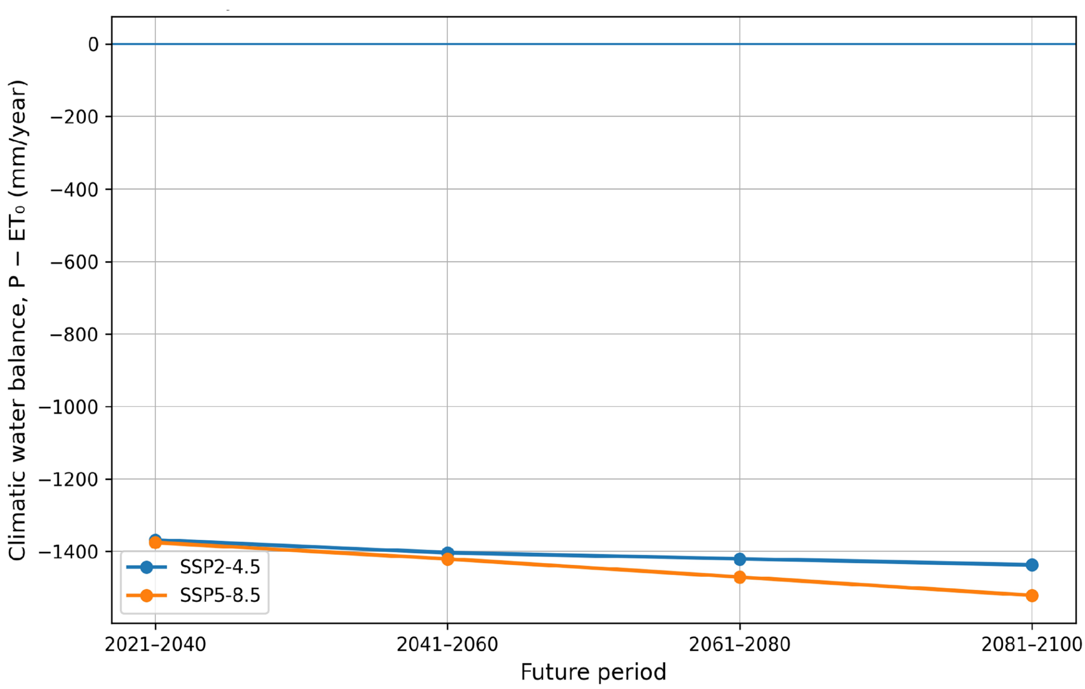

Figure 11. Projected climatic water balance, calculated as precipitation minus ET_0, under SSP2-4.5 and SSP5-8.5. Negative values indicate increasing atmospheric moisture deficit.

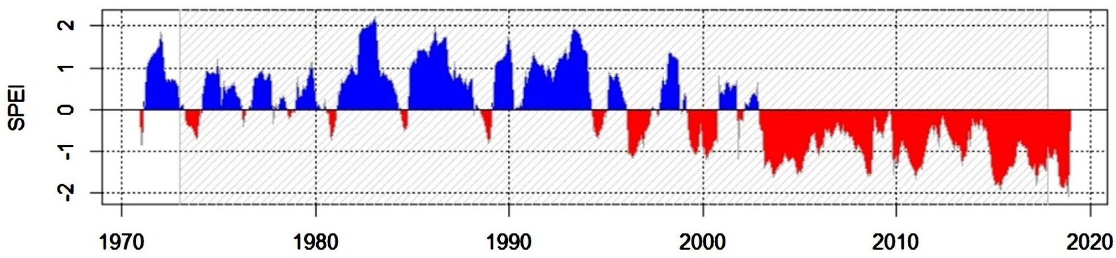

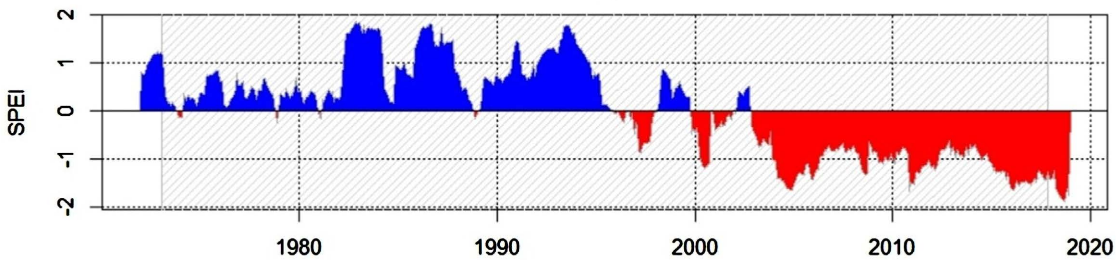

Figure 12. The SPEI in the Al-Madinah region from 1970 to 2018 at 12-month (above) and 24-month (bottom). *Red color represented drought situations with negative values, and blue color symbolized wet conditions with positive values.

and severe wet conditions covering most parts of Saudi Arabia in the period 1985 to 1997, with fluctuations and frequent dry conditions from 1999 until 2018. Amin et al. (2016) also confirmed that the KSA experienced extreme drought events from (January) 2000 to (July) 2013 using the SPI index, whereas Almazroui (2019) concluded that applying the SPI index from 1978 to 2017 indicated that the drought occurred typically from June to September in Saudi Arabia, as well as October despite it being a transition month, October experienced drought conditions for around 29 years out of 40 years used in the study.

The SPEI projections (**Figure 13**) showed a clear temporal shift in hydroclimatic conditions under both emission scenarios. Conditions shifted from comparatively moist in the early to mid-21st century to progressively arid after mid-century. Drought intensification became most pronounced in the late-century period, especially after 2080. Compared with SSP2-4.5, SSP5-8.5 showed a stronger and more persistent drought signal, consistent with the anticipated impact of elevated greenhouse gas forcing on evapotranspiration demand and water deficits. Overall, the findings indicate that drought risk is expected to rise significantly by the end of the century, particularly under the high-emission SSP5-8.5 scenario. These findings agree with the United Nations (2015) report about extreme climate indices for the Arab region, pointing to the dry periods increasing by the end of the century, particularly in the western and northern parts of the Arabian Peninsula. Moreover, according to MEIMR (2016), the more vulnerable areas to desertification by 2080 are expected to be in the regions in the northwest of Saudi Arabia, where Al-Madinah is located.

The use of WorldClim data provided a consistent and accessible basis for estimating reference evapotranspiration (ET_0) across the study area, particularly

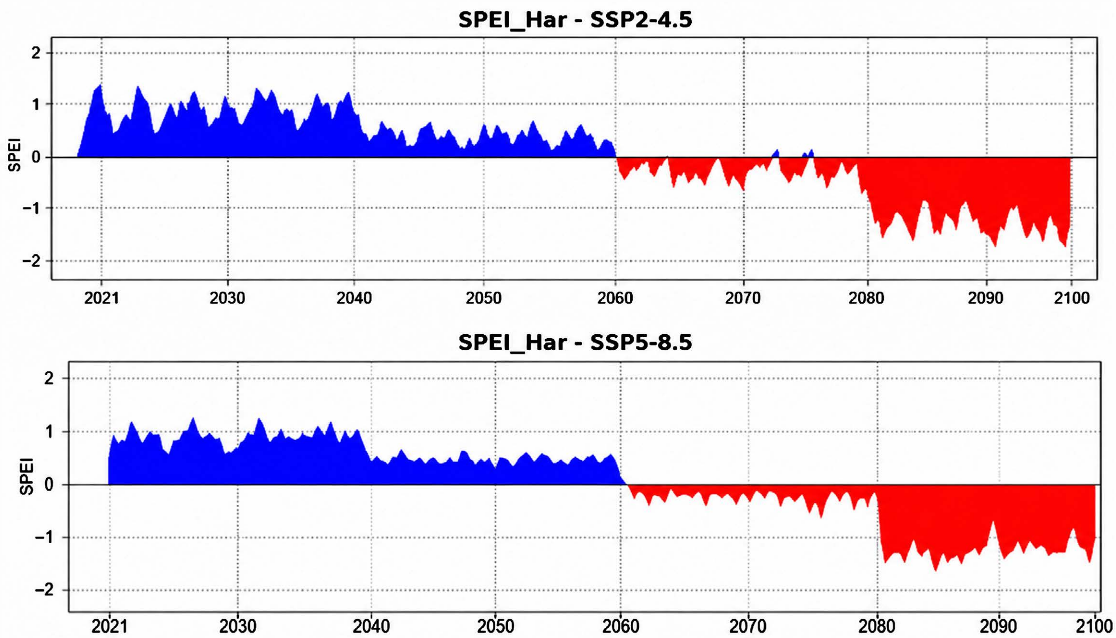

Figure 13. The SPEI in the Al-Madinah region under SSP2-4.5 and SSP5-8.5 scenarios.

where long-term and spatially distributed station observations are limited. However, because WorldClim is a gridded climate dataset, the derived ET_0 values should be interpreted as spatial estimates rather than direct field measurements. Although this study validated WorldClim-derived Hargreaves ET_0 against station-based FAO-56 Penman-Monteith and station-based Hargreaves ET_0, uncertainty may remain due to spatial interpolation, local topographic effects, and differences between gridded and point-based observations. Future work could further improve the assessment by incorporating additional meteorological stations, observed evapotranspiration records where available, and other gridded or remotely sensed climate datasets. This would help refine the spatial patterns of ET_0 and increase confidence in future drought and evapotranspiration projections.

4. Conclusion

The results demonstrated that WorldClim climate data provide a useful basis for ET_0 estimation in the Al-Madinah region, particularly where long-term station data are limited or spatially sparse. The comparison between WorldClim and observed station temperature records showed very strong agreement for Tmax, Tmin, Tmean, and precipitation, indicating that WorldClim successfully captured the seasonal climate patterns in the study area. However, the error assessment identified a slight underestimation of temperature values, particularly in maximum temperature, which should be considered when estimating and mapping climate variables.

The validation of WorldClim-derived Hargreaves ET_0 against station-based FAO-56 Penman-Monteith and station-based Hargreaves ET_0 further supported the suitability of the dataset for representing seasonal ET_0 variability. Future projections indicated a consistent increase in evapotranspiration ET_0 across all periods and scenarios, with more pronounced changes under the high-emission SSP5-8.5 scenario. Although precipitation is projected to increase moderately in some future periods, the increase is insufficient to offset the stronger rise in ET_0. Consequently, the climatic water balance becomes increasingly negative, explaining the projected intensification of SPEI-based drought conditions.

The study highlighted the value of WorldClim-based climate projections and geospatial analysis for assessing evapotranspiration, climatic water balance, and drought susceptibility in arid and semi-arid regions. These would provide useful spatial information for understanding future climate-change impacts, supporting water-resource planning, and improving drought-risk assessment in the Al-Madinah region.

Conflicts of Interest

The author declares no conflicts of interest regarding the publication of this paper.

References

Abdullah, H. M. (2014). Standardized Precipitation Evapotranspiration Index (SPEI) Based Drought Assessment in Bangladesh. In *Proceedings of 5th International Conference on Environmental Aspects of Bangladesh* (pp. 40-42). Bangladesh Environment Network Japan Chapter.

Ahmed, K., Sachindra, D. A., Shahid, S., Iqbal, Z., Nawaz, N., & Khan, N. (2020). Multi-Model Ensemble Predictions of Precipitation and Temperature Using Machine Learning Algorithms. *Atmospheric Research, 236,* Article ID: 104806. https://doi.org/10.1016/j.atmosres.2019.104806

Alharbi, O. (2024). *GIS-Based Modelling of Shallow Groundwater Potential in Arid Regions under Changing Climate and Future Water Demands: A Case Study of Al-Madinah, Saudi Arabia.* Ph.D. Thesis, University of York.

Almazroui, M. (2019). Assessment of Meteorological Droughts over Saudi Arabia Using Surface Rainfall Observations during the Period 1978-2017. *Arabian Journal of Geosciences, 12,* Article No. 694. https://doi.org/10.1007/s12517-019-4866-2

Almazroui, M., Islam, M. N., Saeed, S., Saeed, F., & Ismail, M. (2020). Future Changes in Climate over the Arabian Peninsula Based on CMIP6 Multimodel Simulations. *Earth Systems and Environment, 4,* 611-630. https://doi.org/10.1007/s41748-020-00183-5

AL-Shaibani, A. M., Lloyd, J., Abokhodair, A. A., & Al-Ahmari, A. (2007). A Hydrogeological and Quantitative Groundwater Assessment of the Basaltic Aquifer, Northern Harrat Rahat, Saudi Arabia. *Arab Gulf Journal of Scientific Research, 25,* 39-49.

Amin, M. T., Mahmoud, S. H., & Alazba, A. A. (2016). Observations, Projections and Impacts of Climate Change on Water Resources in Arabian Peninsula: Current and Future Scenarios. *Environmental Earth Sciences, 75,* Article No. 864. https://doi.org/10.1007/s12665-016-5684-4

Bastidas Osejo, B., Betancur Vargas, T., & Alejandro Martinez, J. (2019). Spatial Distribution of Precipitation and Evapotranspiration Estimates from WorldClim and Chelsa Datasets: Improving Long-Term Water Balance at the Watershed-Scale in the Urabá Region of Colombia. *International Journal of Sustainable Development and Planning, 14,* 105-117. https://doi.org/10.2495/sdp-v14-n2-105-117

Čadro, S., Uzunović, M., Žurovec, J., & Žurovec, O. (2017). Validation and Calibration of Various Reference Evapotranspiration Alternative Methods under the Climate Conditions of Bosnia and Herzegovina. *International Soil and Water Conservation Research, 5,* 309-324. https://doi.org/10.1016/j.iswcr.2017.07.002

Delgado-Ramírez, G., Bolaños-González, M. A., Quevedo-Nolasco, A., López-Pérez, A., & Estrada-Ávalos, J. (2023). Estimation of Reference Evapotranspiration in a Semi-Arid Region of Mexico. *Sensors, 23,* Article 7007. https://doi.org/10.3390/s23157007

Driouech, F., ElRhaz, K., Moufouma-Okia, W., Arjdal, K., & Balhane, S. (2020). Assessing Future Changes of Climate Extreme Events in the CORDEX-MENA Region Using Regional Climate Model Aladin-Climate. *Earth Systems and Environment, 4,* 477-492. https://doi.org/10.1007/s41748-020-00169-3

Elnesr, M., & Alazb, A. (2013). Effect of Climate Change on Spatio-Temporal Variability and Trends of Evapotranspiration, and Its Impact on Water Resources Management in the Kingdom of Saudi Arabia. In B. R. Singh (Ed.), *Climate Change—Realities, Impacts over Ice Cap, Sea Level and Risks*. InTech. https://doi.org/10.5772/54832

ElNesr, M., Alazba, A., & Abu-Zreig, M. (2010). Spatio-Temporal Variability of Evapotranspiration over the Kingdom of Saudi Arabia. *Applied Engineering in Agriculture, 26,* 833-842. https://doi.org/10.13031/2013.34944

Ezz, H., & Abdelwares, M. (2025). Quantifying Eto Maps across Egypt: A Remote Sensing Approach to Address Water Needs for Agricultural Irrigation. *Engineering Research: Perspectives on Recent Advances, 4,* 129-145. https://doi.org/10.9734/bpi/erpra/v4/4303

Faye, C., Grippa, M., & Wood, S. (2019). Use of the Standardized Precipitation and Evapotranspiration Index (SPEI) from 1950 to 2018 to Determine Drought Trends in the Senegalese Territory. *Climate Change, 5,* 327-341.

Feng, G., Cobb, S., Abdo, Z., Fisher, D. K., Ouyang, Y., Adeli, A. et al. (2016). Trend Analysis and Forecast of Precipitation, Reference Evapotranspiration, and Rainfall Deficit in the Blackland Prairie of Eastern Mississippi. *Journal of Applied Meteorology and Climatology, 55,* 1425-1439. https://doi.org/10.1175/jamc-d-15-0265.1

Fick, S. E., & Hijmans, R. J. (2017). WorldClim 2: New 1-km Spatial Resolution Climate Surfaces for Global Land Areas. *International Journal of Climatology, 37,* 4302-4315. https://doi.org/10.1002/joc.5086

Fisher, D. K., & Pringle III, H. C. (2013). Evaluation of Alternative Methods for Estimating Reference Evapotranspiration. *Agricultural Sciences, 4,* 51-60. https://doi.org/10.4236/as.2013.48a008

GASTAT (2010). *Population & Housing Census.* Saudi Central Department of Statistics and Information, Ministry of Economy and Planning, Kingdom of Saudi Arabia. https://www.stats.gov.sa/en/statistics-tabs?tab=436312&category=1340083

Gharbia, S. S., Smullen, T., Gill, L., Johnston, P., & Pilla, F. (2018). Spatially Distributed Potential Evapotranspiration Modeling and Climate Projections. *Science of the Total Environment, 633,* 571-592. https://doi.org/10.1016/j.scitotenv.2018.03.208

Gutub, S. A. (2013). A Case Study of Al-Madinah's Water Resources and Reclaimed Wastewater Reuse Perspective. *International Journal of Civil & Environmental Engineering IJCEE-IJENS, 13,* 9-16.

Harris, I., Jones, P. D., Osborn, T. J., & Lister, D. H. (2014). Updated High-Resolution Grids of Monthly Climatic Observations—The CRU TS3.10 Dataset. *International Journal of Climatology, 34,* 623-642. https://doi.org/10.1002/joc.3711

Hodam, S., Sarkar, S., Marak, A. G. R., Bandyopadhyay, A., & Bhadra, A. (2017). Spatial Interpolation of Reference Evapotranspiration in India: Comparison of IDW and Kriging

Methods. *Journal of The Institution of Engineers (India): Series A, 98,* 511-524. https://doi.org/10.1007/s40030-017-0241-z

Hodson, T. O. (2022). Root-Mean-Square Error (RMSE) or Mean Absolute Error (MAE): When to Use Them or Not. *Geoscientific Model Development, 15,* 5481-5487. https://doi.org/10.5194/gmd-15-5481-2022

Jose, D. M., Vincent, A. M., & Dwarakish, G. S. (2022). Improving Multiple Model Ensemble Predictions of Daily Precipitation and Temperature through Machine Learning Techniques. *Scientific Reports, 12,* Article No. 4678. https://doi.org/10.1038/s41598-022-08786-w

Lemenkova, P. (2022). Evapotranspiration, Vapour Pressure and Climatic Water Deficit in Ethiopia Mapped Using GMT and Terraclimate Dataset. *Journal of Water and Land Development, No. 54,* 201-209. https://doi.org/10.24425/jwld.2022.141573

Mahmoud, S. H., & Alazba, A. A. (2016). A Coupled Remote Sensing and the Surface Energy Balance Based Algorithms to Estimate Actual Evapotranspiration over the Western and Southern Regions of Saudi Arabia. *Journal of Asian Earth Sciences, 124,* 269-283. https://doi.org/10.1016/j.jseaes.2016.05.012

Mahmoud, S. H., & Gan, T. Y. (2019). Irrigation Water Management in Arid Regions of Middle East: Assessing Spatio-Temporal Variation of Actual Evapotranspiration through Remote Sensing Techniques and Meteorological Data. *Agricultural Water Management, 212,* 35-47. https://doi.org/10.1016/j.agwat.2018.08.040

Mckee, T. B., Doesken, N. J., & Kleist, J. (1993). The Relationship of Drought Frequency and Duration to Time Scales. In *8th Conference on Applied Climatology* (pp. 179-186) American Meteorological Society.

McSweeney, C. F., Jones, R. G., Lee, R. W., & Rowell, D. P. (2014). Selecting CMIP5 GCMs for Downscaling over Multiple Regions. *Climate Dynamics, 44,* 3237-3260. https://doi.org/10.1007/s00382-014-2418-8

MEIMR (2016). *The Third National Communication (TNC): Report to the United Nations Framework Convention on Climate Change.* Ministry of Energy, Industry and Mineral Resources.

Mohammed, W. E., & Algarni, S. (2020). A Remote Sensing Study of Spatiotemporal Variations in Drought Conditions in Northern Asir, Saudi Arabia. *Environmental Monitoring and Assessment, 192,* Article No. 784. https://doi.org/10.1007/s10661-020-08771-8

Moratiel, R., Bravo, R., Saa, A., Tarquis, A. M., & Almorox, J. (2020). Estimation of Evapotranspiration by the Food and Agricultural Organization of the United Nations (FAO) Penman-Monteith Temperature (PMT) and Hargreaves-Samani (HS) Models under Temporal and Spatial Criteria—A Case Study in Duero Basin (Spain). *Natural Hazards and Earth System Sciences, 20,* 859-875. https://doi.org/10.5194/nhess-20-859-2020

NCM (2019). *Drought Status Analysis.* The National Centre of Meteorology in Saudi Arabia. https://www.ncm.gov.sa/en/the-climate/drought-monitoring/drought-status-analysis

Nooni, I. K., Ogou, F. K., Chaibou, A. A. S., Nakoty, F. M., Gnitou, G. T., & Lu, J. (2023). Evaluating CMIP6 Historical Mean Precipitation over Africa and the Arabian Peninsula against Satellite-Based Observation. *Atmosphere, 14,* Article 607. https://doi.org/10.3390/atmos14030607

Pei, Z., Fang, S., Wang, L., & Yang, W. (2020). Comparative Analysis of Drought Indicated by the SPI and SPEI at Various Timescales in Inner Mongolia, China. *Water, 12,* Article 1925. https://doi.org/10.3390/w12071925

Profillidis, V. A., & Botzoris, G. N. (2019). Statistical Methods for Transport Demand Modeling. In V. A. Profillidis, & G. N. Botzoris (Eds.), *Modeling of Transport Demand* (pp.

163-224). Elsevier. https://doi.org/10.1016/b978-0-12-811513-8.00005-4

Qaisrani, Z. N., Nuthammachot, N., Techato, K., & Asadullah, (2021). Drought Monitoring Based on Standardized Precipitation Index and Standardized Precipitation Evapotranspiration Index in the Arid Zone of Balochistan Province, Pakistan. *Arabian Journal of Geosciences, 14,* Article No. 11. https://doi.org/10.1007/s12517-020-06302-w

Salahudin, H., Shoaib, M., Albano, R., Inam Baig, M. A., Hammad, M., Raza, A. et al. (2023). Using Ensembles of Machine Learning Techniques to Predict Reference Evapotranspiration (ET_0) Using Limited Meteorological Data. *Hydrology, 10,* Article 169. https://doi.org/10.3390/hydrology10080169

Spencer, M. (2013a). *Extraterrestrial Radiation Dataset.* Scottishsnow. https://scottishsnow.wordpress.com/2013/05/20/ext-radiation/

Spencer, M. (2013b). *GB Potential Evapotranspiration Dataset, Extraterrestrial Radiation Dataset.* Scottishsnow. https://scottishsnow.wordpress.com/2013/07/11/gb-pe/

Subyani, A. M., & Al-Ahmadi, F. S. (2011). Rainfall-Runoff Modeling in the Al-Madinah Area of Western Saudi Arabia. *Journal of Environmental Hydrology, 19*. http://www.hydroweb.com/protect/pubs/jeh/jeh2011/subyani2.pdf

Tarawneh, Q., & Chowdhury, S. (2018). Trends of Climate Change in Saudi Arabia: Implications on Water Resources. *Climate, 6,* Article 8. https://doi.org/10.3390/cli6010008

United Nations (2015). *Climate Projections and Extreme Climate Indices for the Arab Region.* https://www.unescwa.org/sites/default/files/pubs/pdf/climate-projections-extreme-climate-indices-arab-region-english.pdf

Vicente-Serrano, S. M., Beguería, S., & López-Moreno, J. I. (2010). A Multiscalar Drought Index Sensitive to Global Warming: The Standardized Precipitation Evapotranspiration Index. *Journal of Climate, 23,* 1696-1718. https://doi.org/10.1175/2009jcli2909.1

WorldClim (2020a). *Global Climate and Weather Data.* https://www.worldclim.org/data/index.html

WorldClim (2020b). *Global Climate Data (WORLDCLIM).* https://www.worldclim.org/

Zhang, J., Bai, Y., Yan, H., Guo, H., Yang, S., & Wang, J. (2020). Linking Observation, Modelling and Satellite-Based Estimation of Global Land Evapotranspiration. *Big Earth Data, 4,* 94-127. https://doi.org/10.1080/20964471.2020.1743612

Appendix

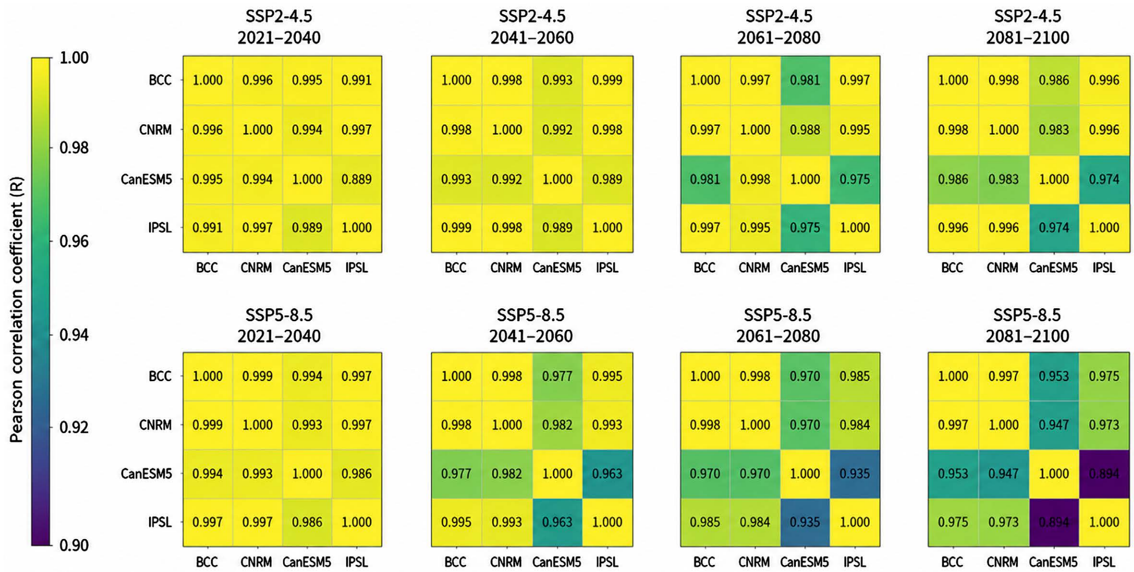

Figure A1. Pairwise correlation heatmaps of projected monthly Hargreaves ET_0 among the four selected CMIP6 GCMs under SSP2-4.5 and SSP5-8.5. Each panel represents one future period: 2021-2040, 2041-2060, 2061-2080, and 2081-2100. Correlation coefficients were calculated using the 12 monthly ET_0 values for each scenario-period combination. Values close to 1 indicate strong agreement among the GCMs in reproducing the seasonal ET_0 pattern.

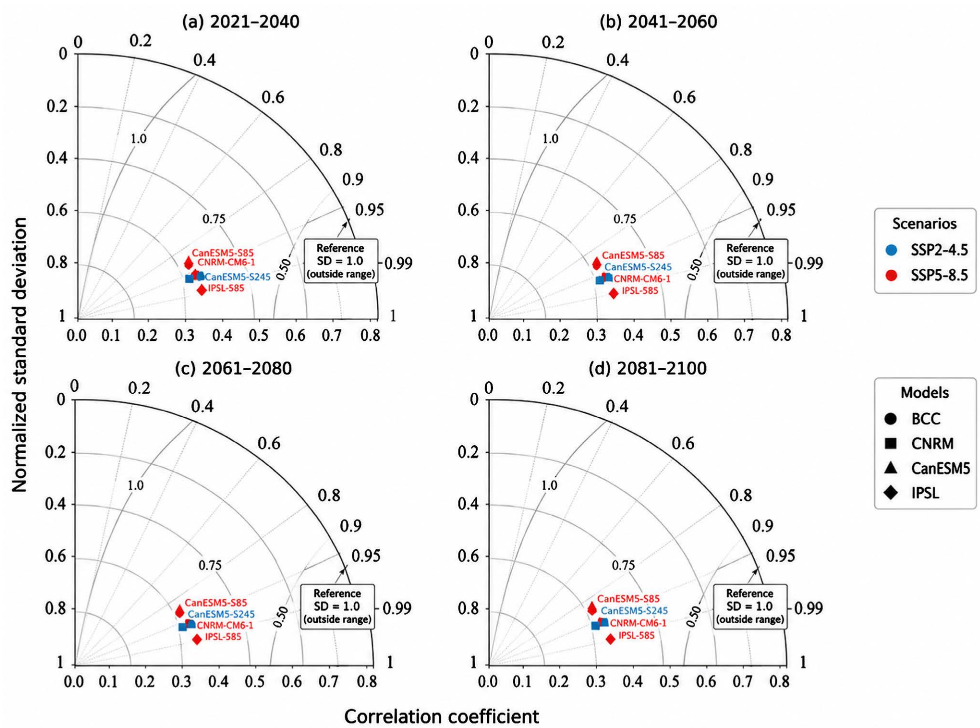

Figure A2. Taylor diagrams comparing projected monthly reference evapotranspiration (ET_0) from four CMIP6 GCMs with the historical WorldClim-derived ET_0 baseline for four future periods under SSP2-4.5 and SSP5-8.5. The radial axis represents the normalized standard deviation, while the angular axis represents the correlation coefficient. The historical reference standard deviation equals 1.0 and lies outside the zoomed axis range. Lower spread among points indicates stronger inter-model consistency.

Table A1. Inter-model spread of projected annual Hargreaves ET_0 among the four selected CMIP6 GCMs under SSP2-4.5 and SSP5-8.5. The coefficient of variation was calculated from the standard deviation and ensemble mean of annual ET_0 across the four GCMs for each scenario and future period.

Scenario	Period	SD mm/year	CV %
SSP2-4.5	2021-2040	29.250	2.012
SSP2-4.5	2041-2060	33.911	2.279
SSP2-4.5	2061-2080	35.763	2.378
SSP2-4.5	2081-2100	30.067	1.976
SSP5-8.5	2021-2040	30.887	2.115
SSP5-8.5	2041-2060	47.083	3.127
SSP5-8.5	2061-2080	58.799	3.777
SSP5-8.5	2081-2100	70.947	4.411